Received: 8 November 2019 | Revised: 31 December 2019 | Accepted: 7 January 2020

DOI: 10.1111/gcbb.12671

ORIGINAL RESEARCH

GLOBAL CHANGE BIOLOGY BIOENERGY

WILEY

Projections of global and UK bioenergy potential from *Miscanthus* × *giganteus*—Feedstock yield, carbon cycling and electricity generation in the 21st century

Anita Shepherd[1] | **Emma Littleton**[2] | **John Clifton-Brown**[3] | **Mike Martin**[1] | **Astley Hastings**[1]

[1]Institute of Biological and Environmental Sciences, School of Biological Sciences, University of Aberdeen, Aberdeen, UK

[2]College of Life and Environmental Sciences, University of Exeter, Exeter, UK

[3]Institute of Biological, Environmental & Rural Sciences (IBERS), Aberystwyth University, Aberystwyth, UK

Correspondence
Anita Shepherd, Institute of Biological and Environmental Sciences, School of Biological Sciences, University of Aberdeen, 23 St. Machar Drive, Aberdeen, Scotland, AB24 3UU.
Email: anita.shepherd@abdn.ac.uk

Funding information
Natural Environment Research Council, Grant/Award Number: NE/M019691/1 and NE/P019951/1; Engineering and Physical Sciences Research Council

Abstract

In this article, we modify bioenergy model MiscanFor investigating global and UK potentials for *Miscanthus* × *giganteus* as a bioenergy resource for carbon capture in the 21st century under the RCP 2.6 climate scenario using SSP2 land use projections. UK bioenergy land projections begin in the 2040s, 60 year average is 0.47 Mega ha rising to 1.9 Mega ha (2090s). Our projections estimate UK energy generation of 0.09 EJ/year (60 year average) and 0.37 EJ/year (2090s), under stable miscanthus yields of 12 t ha^{-1} $year^{-1}$. We estimate aggregated UK soil carbon (C) increases of 0.09 Mt C/year (60 year average) and 0.14 Mt C/year (2090s) with C capture plus sequestration rate of 2.8 Mt C/year (60 year average) and 10.49 Mt C/year (2090s). Global bioenergy land use begins in 2010, 90 year average is 0.13 Gha rising to 0.19 Gha by the 2090s, miscanthus projections give a 90 year average energy generation of 16 EJ/year, rising to 26.7 EJ/year by the 2090s. The largest national capabilities for yield, energy and C increase are projected to be Brazil and China. Ninety year average global miscanthus yield of 1 Gt/year will be 1.7 Gt/year by the 2090s. Global soil C sequestration increases less with time, from a century average of 73.6 Mt C/year to 42.9 Mt C/year by the 2090s with C capture plus sequestration rate of 0.54 Gt C/year (60 year average) and 0.81 Gt C/year (2090s). *M. giganteus* could provide just over 5% of the bioenergy requirement by the 2090s to satisfy the RCP 2.6 SSP2 climate scenario. The choice of global land use data introduces a potential source of error. In reality, multiple bioenergy sources will be used, best suited to local conditions, but results highlight global requirements for development in bioenergy crops, infrastructure and support.

KEYWORDS

bioenergy, carbon, climate change, crop yield, energy generation, land use, MiscanFor, miscanthus, modelling, RCP 2.6

1 | INTRODUCTION

As a bioenergy crop, *Miscanthus* × *giganteus* (*M* × *g*) is an obvious choice for growers. It thrives on poor soils; it requires few farm operations except annual harvest. It can use existing farm machinery and skills, it withdraws nutrients into the rhizome at senescence to be reused the following season and has a high water efficiency compared to other arable crops (McCalmont et al., 2017). As such, it can thrive on waste land, or poor agricultural soils which provide insufficient economic returns for food crops. After planting, no tillage is required, and mature rhizomes require no fertilizer; hence, the greenhouse gas (GHG) emission from this crop is low compared to arable crops and intensive grassland. McCalmont et al. (2017) state that with an offtake of 10–15 t DM ha^{-1} $year^{-1}$, the organic N in harvest material taken from a site would range between 49 and 73.5 kg N/ha. Accounting for an atmospheric N deposition rate of 35–50 kg N ha^{-1} $year^{-1}$ (Goulding et al., 1998), McCalmont et al. suggest that miscanthus is unlikely to benefit greatly from inputs of N unless it was being established in very low fertility soils; hence, we have assumed this to be true for the majority of global bioenergy crops that no nutrients are needed after the first 2 years rhizome growth.

Biomass from miscanthus is considered a C-neutral resource whether or not the soil C stocks increase (Robertson et al., 2017) that can be burnt for heat, electricity or combined heat and power in localized energy plants, with or without C capture and storage (CCS). Its potential to increase soil C and the potential for CCS make it all the more advantageous as a fuel in a climate requiring mitigation of carbon dioxide (CO_2). Rising prices of oil and gas and cost reductions in the production of bioenergy systems increased the competitiveness of biomass for energy use in the early 2000s (Schlamadinger, Faaij, Junginger, Daugherty, & Woess-Gallasch, 2006), but recent technology advances in shale hydrocarbon extraction have reduced the price of oil and gas and this advantage. However, the urgency of climate mitigation makes this an important resource as a C neutral fuel. Perennial miscanthus has energy output/input ratios 10 times higher (McCalmont et al., 2017) than annual crops used for energy, the total C cost of energy production is 20–30 times lower than fossil fuels and N_2O emissions can be five times lower under unfertilized miscanthus than annual crops and up to 100 times lower than intensive pasture.

MiscanFor (Hastings, Clifton-Brown, Wattenbach, Mitchell, & Smith, 2009) is a model which provides projections of bioenergy crop growth and power generation (developed from the MISCANMOD model of Clifton-Brown et al., 2001). It can be tailored to various crops, including *M* × *g*. It is a daily mechanistic simulation requiring soil and climate databases, and outputs average annual values on a grid point basis globally. Input is facilitated via a Java interface, and output supplied in the form of data files and plots. The MiscanFor model is process-based mixed with empirical components. An overview of the model before we modified it can be seen in Figure 1.

The original model before we added capability is a working model providing crop yield, power generation and environmental variables, and the following is a description of the pre-modified model.

Dry matter assimilation is calculated from the fraction of radiation intercepted by the canopy (dependant on leaf area index [LAI], an extinction coefficient and photosynthetically active radiation), modified by radiation use efficiency and an overheating factor.

MiscanFor includes crop growth parameters for *M* × *g*. The model has an accounting mechanism for persistent high soil water deficit and low temperature thresholds which kill the crop (60 days below −7°C and 60 days below permanent wilting point). MiscanFor reduces assimilate (also known as photosynthate) production over a leaf temperature threshold of 28°C. Both the increase and senescent decline of LAI are linearly related to the degree day accumulation above a threshold value. There are six phenological stages of crop development and senescence: rhizome dormancy, shoot development, leaf development, leaf senescence, plant senescence, and peak harvest. These stages are determined by reaching degree day thresholds and can be triggered by environmental events such as drought and temperature thresholds and frost occurrence.

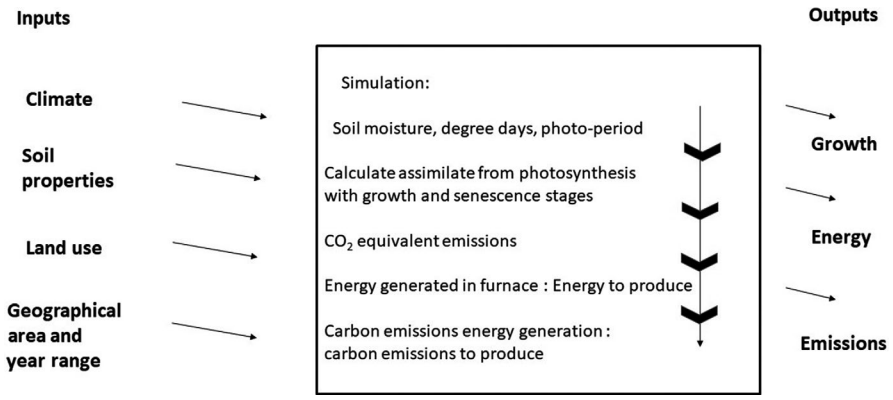

FIGURE 1 MiscanFor model before modification

Average annual crop yields of dry matter biomass include years of zero crop yield when crops are drought- or frost-killed. Hence, crops in a hostile environment will show a lower average yield, even if some years obtain high yields, in order to make realistic predictions and not generate unrealistic expectations for the growers and energy industry.

MiscanFor includes GHG emission and energy cost calculations, based on Sims, Hastings, Schlamadinger, Taylor, and Smith (2006), Clifton-Brown, Breuer, and Jones (2007), St Clair, Hillier, and Smith (2008) and Hastings et al. (2008). It calculates a life cycle analysis of C cost from anthropogenic energy and CO_2-C equivalent emission using an internal database of global coefficients for ground preparation, machinery and initial rhizome production. Soil CO_2-C equivalent emissions are calculated from the difference between initial soil C at the time of crop establishment and the estimated soil organic carbon (SOC) at the end of the crop cycle. Net energy generated is the energy generated minus latent heat and the energy cost of feedstock production.

MiscanFor uses the global International Geosphere-Biosphere Programme (IGBP) soil and land use parameters database (Global Soil Data Task Group, 2000) at a resolution of 5 × 5 arc minutes. It has also used the HSWD soil data on a 30 × 30 arc-second grid in Hastings et al. (2014). It uses the Climate Research Unit Time Series (CRU TS) 4.01 climate data for 1901–2016 (Harris & Jones, 2017), HADCM3 A1F1, A2, B1 and B2 2000–2010, and the UK Climate Projections 2009 (UKCP09) global climate projections (UKCP09, 2018) for 2001–2100, all at 0.5° scale. MiscanFor has previously been successfully tested against yield observations from across the United Kingdom, China, Japan and Korea and Europe (Hastings et al., 2009).

Hastings et al. (2008) reported overestimations at lower latitudes and arid climates. A modification of photosynthetic production with climate is required. In addition, MiscanFor is sensitive to climate parameters creating vulnerability to drought (Pogson, Hastings, & Smith, 2012). Both these issues have been traced back to crop and water processes. New databases available can provide parameters which will allow for updates on processes.

RCP 2.6 (IPCC, 2014) is a greenhouse gas trajectory based on an IPCC socio-economic pathway which limits global warming to 2°C and assumes an increasing reliance on Bioenergy with Carbon Capture and Storage (BECCS). It is estimated that BECCS will produce global electricity generation of up to 300 EJ/year (Rogelj et al., 2015) and store 616 Gt CO_2 (Mander, Andersona, Larkin, Gough, & Vaughan, 2016) cumulatively by 2100. In order to check what a contribution a bioenergy feedstock can make to this figure, we need a reliable projection of bioenergy feedstock yield for energy production C accounting, and for this, we need a robust model for bioenergy. Our remit is to further enhance the MiscanFor model, in order to assess the global contribution potential of miscanthus bioenergy to RCP 2.6 requirements using only $M \times g$ as a feedstock.

RCP 2.6 assumes that global annual GHG emissions peak between 2010 and 2020, with emissions declining substantially afterwards (Meinshausen et al., 2011) due to C mitigation measures. The RCP 2.6 scenario can use Shared Socio-economic Pathways known as SSPs (Riahi et al., 2017) which provide flexible descriptions of possible futures within each RCP. MiscanFor does not calculate land use; it requires it as an input. Integrated assessment models (IAMs) can calculate land use projections accounting for the SSP requirements, involving demographic, technological, economic, social, cultural and political interactions. In this study, we have used published global gridded bioenergy land use data for SSP2 projections (van Vuuren et al., 2011, 2017), which have been reviewed by Vaughan et al. (2018) as being ambitious but consistent with current relevant literature with respect to assumed biomass resource and land use.

2 | METHODS AND MATERIALS

See Table 1 for a list of the acronyms used throughout this article.

2.1 | MiscanFor modification

We have updated MiscanFor and extended its capability in a variety of ways (Figure 2), to include new land use and climate databases, an extended interface, addition of a soil C and litter decomposition module, updating the evapotranspiration method, modified downregulation of stress-related assimilate production, added groundwater support and adiabatic temperature modification.

Step 1: The MiscanFor soil database has been modified to use either the global IGBP soil database at a resolution of 5 × 5 arc minutes (global or continental simulations) or the Harmonized World Soil Database (HWSD) global soil database (Wieder, Boehnert, Bonan, & Langseth, 2014) currently implemented for the United Kingdom at a resolution of 30 × 30 arc-seconds (national or regional simulations).

Step 2: Climate scenarios have been updated to use the IPCC RCP 2.6 SSP2 climate and social development pathway (IPCC, 2007). Climate projections covering the years 2006–2099, corresponding to this pathway, were produced from the Met Office Hadley Centre climate model HadGEM2-ES (Collins et al., 2011; Martin et al., 2011). These data were downscaled to 0.5° and bias-corrected to calibrate with WATCH observed climatology over 1960–1999 (Hempel, Frieler, Warszawski, Schewe, & Piontek, 2013).

Step 3: We have used van Vuuren et al. (2017) gridded bioenergy land use for SSP2 projections as input data to

TABLE 1 Acronyms

Acronym	Full name/description
IPCC	Inter-governmental Panel on Climate Change
RCPs	Representative Concentration Pathways, greenhouse gas concentration trajectories
RCP 2.6	Climate projection commonly referred to under the same name as its RCP
SSP2	Shared Socio-economic Pathway
BECCS	Bioenergy with Carbon Capture and Storage
CCS	Carbon Capture and Storage
GGR	Greenhouse Gas Reduction
GHG	Greenhouse Gas
CO_2-C	Carbon dioxide mass in terms of its carbon only
CRU	Climate Research Unit at University of East Anglia
TS4.01	Time-Series (TS) vsn 4.01 of high-resolution gridded historical climate data
HadGEM2-ES	Hadley Centre climate model providing RCP2.6 climate projection
HADCM3	Older Hadley Centre climate model
MiscanFor	Bioenergy crop yield, environmental and power generation model
IAM	Integrated Assessment Model
IMAGE	Integrated assessment model which provided land use input data for this study
GUI	Graphic user interface, the front and visible part of a model
IGBP	International Geosphere-Biosphere Programme 5 arc min soils database used
HWSD	Harmonized World Soils Database 30 arc sec soils database used
M × *g*	*Miscanthus* × *giganteus*
RUE	Radiation Use Efficiency, modelling link between photosynthesis and radiation
RUEDR	Radiation Use Efficiency Down-Regulation
TrueDR	Temperature Radiation Use Efficiency Down-Regulation
LeafTDR	Leaf Temperature Down-Regulation
DM Biomass	Dry Matter Biomass, standard biomass measurement without moisture
LAI	Leaf Area Index
Net energy	Power generation output minus energy input to grow crop
EJ	ExaJoule or 1×10^{18} Joules
MJ	MegaJoule or 1×10^{6} Joules
Mha	Mega hectare or 1×10^{6} ha

MiscanFor; this was created for the van Vuuren study by the IMAGE IAM (Stehfest, Van, Vuuren, Kram, & Bouwman, 2014). The bioenergy land use changes through the decades and shows a global increase over the 21st century. SSP2 land use projections for bioenergy are provided from simulations of the IMAGE IAM in the form of a global mask of grid squares at 0.5° (Figure 3) containing a value for the fraction of bioenergy land use through the 21st century (Daioglou, Doelman, Wicke, Faaij, & Vuuren, 2019; Doelman et al., 2018). The SSP2 data also contain the fraction of area per grid square for bioenergy land use. MiscanFor contains the option to either use the SSP2 bioenergy land use or retain the pre-modified version's broader land use from the IGBP database. The IMAGE-derived SSP2 bioenergy data set contains pre-calculated locations of bioenergy land use on a global 0.5° grid. The IGBP land use gives the grassland, arable and built-up land use, and the model allows the user to choose a percentage use of the grassland or arable land replaced by bioenergy crop on a 5 arc minute grid. For this study, we use the SSP2 land use.

Step 4: An extended interface has been created. MiscanFor has a Java graphical user interface (GUI) containing default values which can be edited. The user can set spatial and temporal boundaries, percentage use of bioenergy crops on existing land use, crop growth, environmental, efficiency and economic parameters. Many parameters previously contained within the model are now displayed external and editable in the GUI, notably crop growth parameters, which will allow ease of future simulations of different miscanthus varieties or other crops and trees (Figure 4).

Step 5: We have provided two options to simulate evapotranspiration. The Penman–Monteith (FAO method, Allen, Pereira, Raes, & Smith, 1998) is commonly implemented in crop growth models and requires wind speed, which updated climate projection databases now supply. The CRU TS4.01 provides a Penman–Monteith potential evapotranspiration, but if older CRU historical climate or HADCM3 scenarios are used, they lack wind speed data so the Thornthwaite evapotranspiration calculation is used.

Step 6: We have added groundwater support and adiabatic lapse rate of temperature to national scale, which further discerns differences and enhances spatial resolution. The HWSD soil database is used for national scale and contains groundwater support data. This groundwater classification enables a modification of the initial amount of soil water at the start of each year according to the groundwater category of the data. Elevation data have been obtained from the CGIAR-CSI website (Jarvis, Reuter, Nelson, & Guevara, 2008) and averaged to the spatial resolution of both the soil and climate data. An adiabatic lapse rate for modification of temperature with elevation has been implemented in the national scale data. Otherwise, the model processes are identical to the global version of the model.

Step 7: We have linked photosynthesis to temperature and water deficit. Radiation use efficiency or RUE (Monteith, 1977)

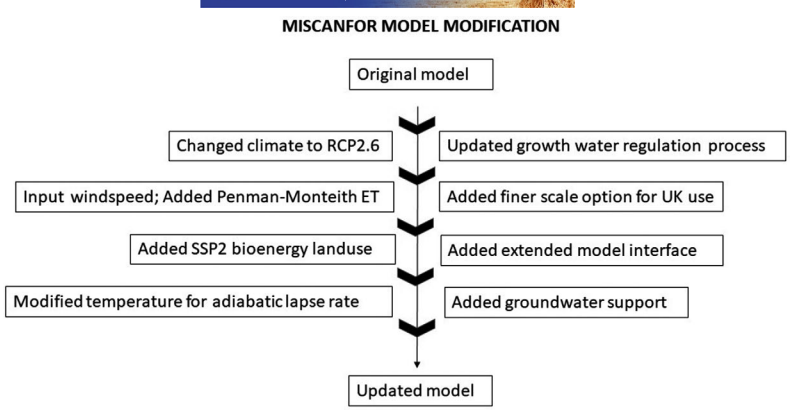

FIGURE 2 Schematic of MiscanFor model modification

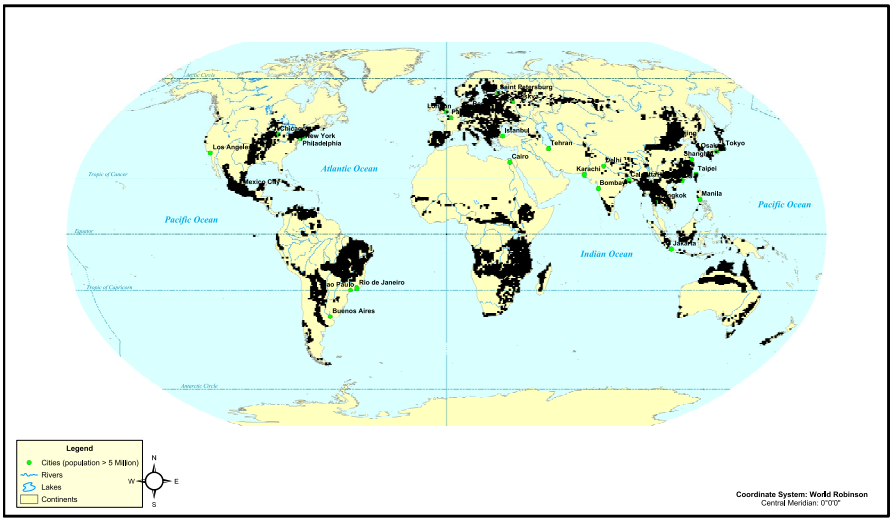

FIGURE 3 Global bioenergy land use, from the IMAGE integrated assessment model

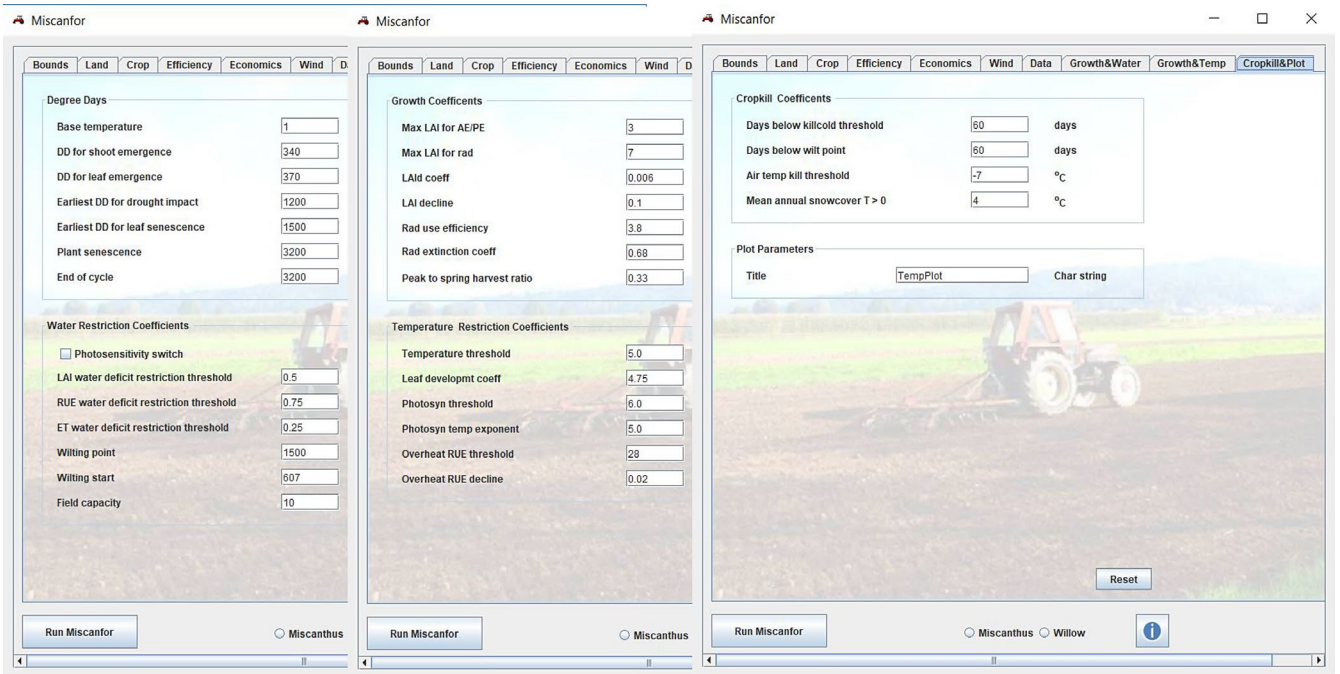

FIGURE 4 The extended MiscanFor interface

quantifies the efficiency of a plant in converting light energy for CO_2 assimilation to biomass. RUE is restricted with lack of an incoming water resource via limits on transpiration, photosynthesis and leaf expansion. Downregulation of RUE has been updated via soil evaporation, photosynthesis temperature and leaf temperature regulation, a method developed from observations in Farage, Blowers, Long, and Baker (2006) on the RUE downregulation function.

$$\mathrm{DMY} = \mathrm{RADintercept} * \mathrm{RUE} * \mathrm{RUEDR} * \mathrm{TrueDR} * \mathrm{LeafTDR}, \quad (1)$$

where DMY is daily assimilate produced (g m^{-2} day^{-1}), RADintercept is daily photosynthetically active radiation (PAR) intercepted by the crop each day (MJ m^{-2} day^{-2}), RUE is in g/MJ of PAR, RUEDR is the daily RUE restriction based on soil water deficit. TrueDR means temperature of RUE downregulation and is the daily downregulation of RUE if leaf temperature is over a maximum temperature threshold. LeafTDR means leaf temperature downregulation and is the daily downregulation of RUE if the temperature during leaf expansion and development is over a maximum threshold. These are our own terms for these parameters, not to be confused with any other existing terms. Together, they have the effect of increasing downregulation during early growth and reducing it at senescence; the lower the latitude, the longer the period of increased downregulation.

Step 8: A new soil C module has been incorporated in this global version of MiscanFor, following successful validation for multiple locations in a site version of MiscanFor (Dondini, Hastings, Saiz, Jones, & Smith, 2009). This module is based on a proposed generic theory for the dynamics of C and nitrogen (N; Bosatta & Agren, 1985, 1991). Algorithms simulate the input of litter or organic material at various time intervals as unique pools of soil organic matter with separate exponential rates for decomposition. Initial soil C is obtained from the soil database. A location producing a greater crop yield, and hence leaf litter, has the potential to increase soil C more than a crop location suffering from drought or frost kill. The amount of litter input to the soil is the difference between miscanthus peak yield and harvest yield. Mean annual soil C change has been added as map output. Simulated soil C change will be compared against experimental measurements.

2.2 | MiscanFor projected data

Step 1: The bioenergy projections were run using every decade of the 21st century since 2010 under the RCP2.6 scenario with SSP2 bioenergy land use masks for the United Kingdom and globally. Global projections used the 5 arc minute IGBP soil database, and the United Kingdom used the 30 arc second HWSD soil database.

Step 2: Baseline historic data used for calibration with measured variables used CRU TS4.01 climate data, and did not assume a land use mask, running data to match individual sampling points.

Step 3: The Penman–Monteith evapotranspiration option was used with climate projections. The historic TS4.01 climate contains pre-calculated Penman–Monteith evapotranspiration data.

Step 4: For the higher resolution of the national scale United Kingdom data, groundwater support data have been used from the HWSD soil database, and adiabatic lapse rate has been applied to temperature data.

Step 5: Miscanthus harvested yield will be compared against experimental plot yields. The experimental plot yields have been corrected for 20% since it is known that experimental plot yields for miscanthus are artificially high due to the environment (regularly fertilized and with no weeds). Lesur-Dumoulin, Lorin, Bazot, Jeuffroy, and Loyce (2016) reported that commercial grower yields were on average 20% lower than experimental plot yields.

Step 6: Whilst the MiscanFor model contains the ability to simulate irrigated crops, the simulations in this study only consider natural rainfall, since miscanthus is a crop that can tolerate dry areas and is assumed grown on land not viable for other crops, so it is assumed the cost of irrigation would be deemed uneconomic for energy crops. To estimate the energy cost of growing, storing and transporting a Miscanthus crop, we applied the calculations for energy yield (Clifton-Brown et al., 2007) and energy costs (Lai, 2004), using the methodology in Hastings et al. (2009) for an 'optimum' scenario. This method simulates a recommended crop management scenario for Miscanthus: local use of the miscanthus as feedstock for combined heat and electricity within 20 km, harvested nutrient replacement with fertilizer application, two pre-emergence applications of herbicide and using rhizome plant propagation.

Step 8: The energy feedstock is miscanthus bales and is calculated as an energy yield of 18 GJ/t of dry matter yield, minus latent heat of vapourization at 2.72 GJ/t of moisture content (30% of dry matter biomass), minus fixed energy cost (5.64 GJ/year) of crop establishment, minus energy input 0.61 GJ/t per dry matter yield, incorporating fertilizer, harvesting and transport (Hastings et al., 2017). Although contained in the model, this is a chosen option for the projections since the values can be changed for other feedstock processing scenarios.

Step 9: We have calculated the C potential for CCS following Albanito et al. (2019). This is an assumption of 90% CO_2 capture post-combustion at biomass electricity plants, and is broadly similar across plants with varying efficiency:

$$\mathrm{CCS} = [\mathrm{DM} \times 0.5] \times 0.9, \quad (2)$$

where CCS is the annual CO_2 captured and transferred into geological storage expressed as units of C (not CO_2), DM is the dry matter miscanthus biomass, and 0.5 assumes 50% C in biomass, and 0.9 refers to 90% CCS efficiency.

3 | RESULTS

3.1 | Updates concerning soil water

The fine-scale HWSD and coarse-scale IGBP soil databases (used for national and global scale simulations, respectively) were compared for available water capacity (AWC) over the United Kingdom. Figure 5a shows absolute AWC values from the HWSD database. To compare which locations differ between databases, Figure 5b shows the AWC from HWSD minus the AWC from the IGBP soils database. Higher AWC in the IGBP database is coloured orange, higher AWC in the HWSD database is coloured green and both colours darken for greater differences.

The addition of the RCP 2.6 climate data set has provided wind speed, allowing the Penman–Monteith evapotranspiration to be implemented. Figure 6a,b displays global mean annual wind speed and crop evapotranspiration (ET_c). The climate variation is reflected in higher than average mean daily evapotranspiration for north-east and South America. Grey map areas reflect either crop kill, in which case all variables cease to be outputted for that location, or else gaps in databases. Since wind and solar radiation are influential on ET_c, Figure 6 displays a similar distribution of ET to solar radiation modified by wind which is higher on mountain ranges and coastal areas.

Addition of the adiabatic lapse rate to temperature, and groundwater support, has produced a contrast between hills and valleys, and given detail to regions (Figure 7). This will refine the aggregated yield values of a region.

3.2 | Miscanthus carbon effects

Favourable comparisons have already been made (Dondini et al., 2009) between measured soil C data simulations resulting from the Bosatta and Agren procedure implemented within another version of MiscanFor. We have used the Bosatta and Agren procedure for litter and soil C pool turnover to show a simulated-observed data comparison shown in

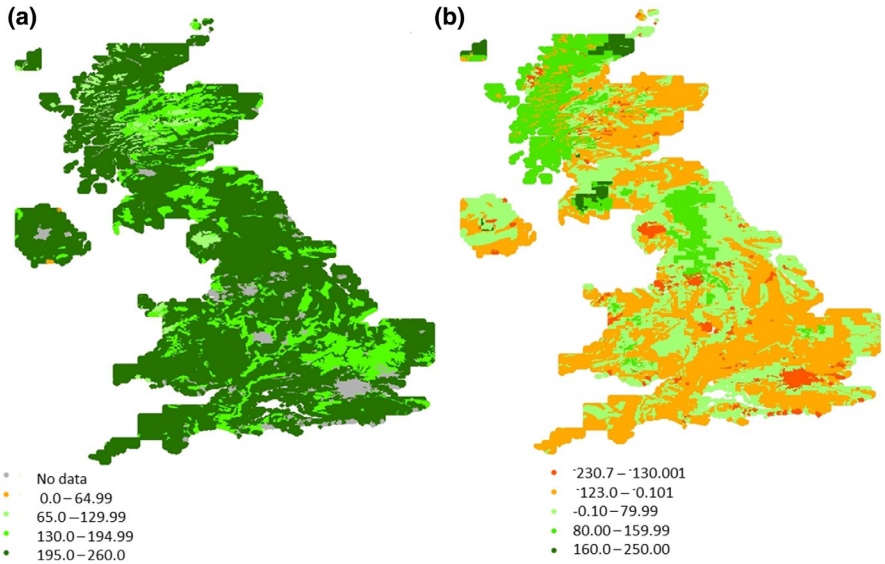

FIGURE 5 Harmonized World Soil Database (HWSD) (a) soil water capacity (mm), (b) HWSD minus International Geosphere-Biosphere Programme water capacity (mm)

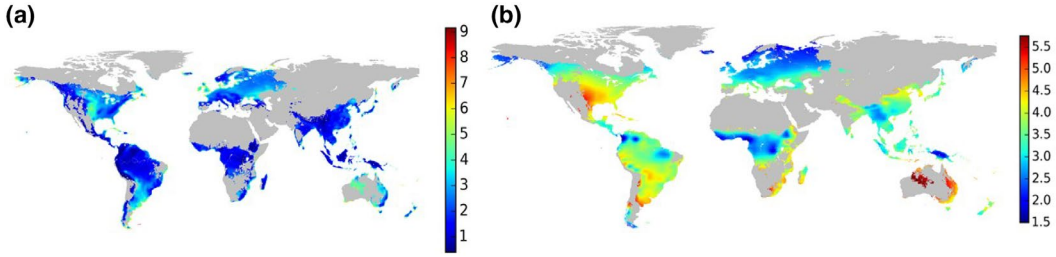

FIGURE 6 Mean daily (a) wind speed (m/s) (b) global evapotranspiration (mm/day) 2070–2090

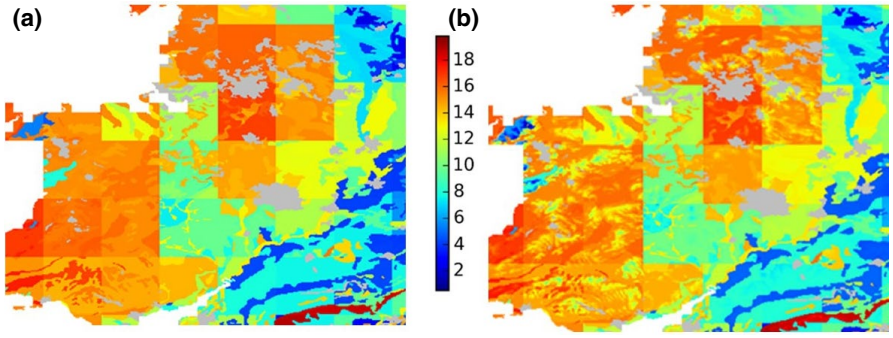

FIGURE 7 Dry matter yield of Miscanthus (t ha^{-1} year^{-1}) Wales and Pennines 2090–2099 (a) without and with (b) adiabatic temperature and groundwater

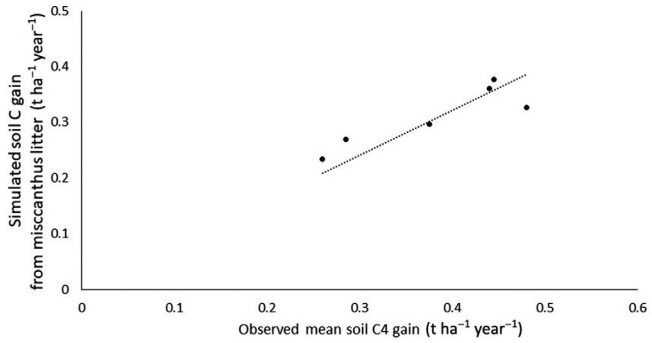

FIGURE 8 Simulated soil carbon change shown against measurements from literature; $R^2 = .59$

Figure 8, using data measurements from a study by Poeplau and Don (2014).

The mean annual soil C change 2010–2019 has been simulated (Figure 9), using the updated MiscanFor at fine scale for the whole of the United Kingdom, and the HWSD database provides the initial soil C. This assumes that a mature miscanthus crop had been grown at that location between 2010 and 2019 and does not take into account existing small urban areas or conversion of land use. Mean annual soil C change (Figure 9) shows contrasts between upland areas (e.g. The Pennines, The Cairngorms), possibly rich in organic matter, which would lose C if ploughed, against lowland agricultural soils (e.g. Staffordshire, Shropshire, Worcestershire) lower in C which could potentially gain soil C under a miscanthus crop.

MiscanFor calculates the soil CO_2 balance (Figure 10) associated with growing the crop to the feedstock delivery (transport and processing CO_2, plus the change in soil CO_2 associated with the new soil C module). If the mean annual soil C has reduced, the mean annual CO_2 emitted will have increased and vice versa. The CO_2 emission resulting from soil C loss is calculated by ratio of molecular weight (IPCC, 2007), and conversely the negative emission associated with soil C gain. The CO_2 emissions (Figure 10) are higher from upland soils, and negative to neutral from lowland agricultural soils. This is assuming a mature miscanthus crop having been grown a number of years, because CO_2-equivalent emission resulting from land use change is not included in the model.

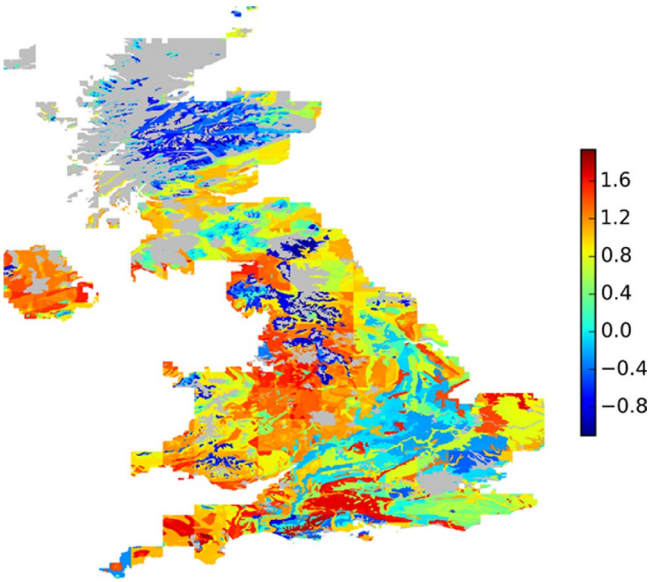

FIGURE 9 Simulation of mean annual soil carbon change (t ha^{-1} year^{-1}) 2010–2019 for United Kingdom under *Miscanthus* × *giganteus*

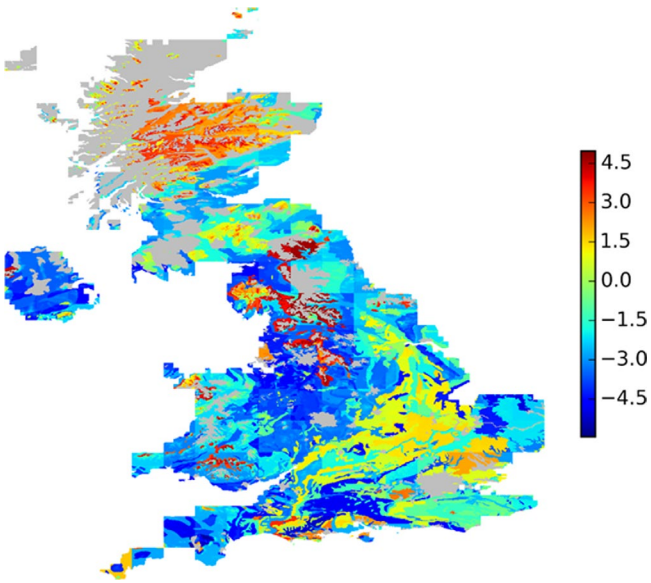

FIGURE 10 Miscanthus CO_2 emission for the UK 2010–2019 (t ha^{-1} year^{-1}; resulting from processing, transport and soil C change)

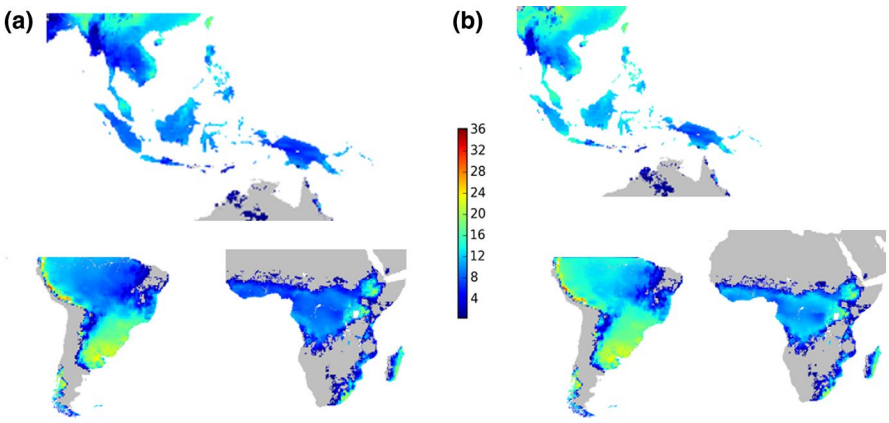

FIGURE 11 Miscanthus dry matter yield, 2090–2099 (t ha^{-1} year^{-1}) (a) with an overheat threshold of 28°C, (b) with an overheat threshold of 35°C

3.3 | Yields and energy generation

A plant overheating factor is integral with the downregulation of photosynthesis. This is known to vary between genotypes of miscanthus (pers. comm. Professor John Clifton-Brown, University of Aberystwyth). $M \times g$ downregulates assimilate production above 28°C, but other genotypes have shown a higher temperature tolerance, for example, *M. sinensis* to 35°C (Hagar, Sinasac, Gedalof, & Newman, 2014). Either yield increase or cropping area expansion (Figure 11) results from changing the overheating temperature threshold from 28 to 35°C. This illustrates the limitation of simulating only $M \times g$, and that in reality other varieties may be best suited to the higher ranges of climate variables.

For the simulated-observed harvest yield data (Figure 12), each simulated value is time and location specific to match with each observed value from collated experimental plot yields (natural rainfed $M \times g$, extracted from Hastings et al., 2009). The experimental plot yields have been corrected for 20% to correct for experimental plot yields being artificially high. Experimental plots often apply fertilizer whereas growers often stop fertilizing a mature crop.

Despite the global simulated-observed yields showing a spread of data, the medium to high yields match satisfactorily ($R^2 = .51$) between 7 and 25 t ha^{-1} year^{-1}. Including yields below 6 t ha^{-1} year^{-1} creates lower correlation ($R^2 = .36$). We believe these data to be juvenile rhizome yields which slowly increase to that of mature plants, whereas MiscanFor assumes mature rhizome yields. Model scale is also influential on the spread of data; the observed data are collated from global experimental plots whereas global simulations use 5 arc minute soil data and 0.5 degree climate data, thereby missing variability at finer detail. We have assumed that for the majority of global bioenergy crops, no nutrients are needed after the first 2 years rhizome growth, this could create an overestimation in global yields for the areas with very poor soil fertility, but regarding Figure 12 since the data come from research plots from various studies, it is unlikely that a spread of data is related to nutrient limitation

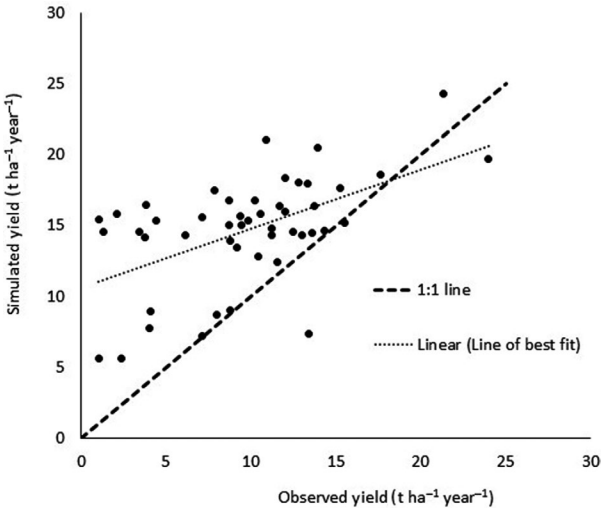

FIGURE 12 Dry matter yield: simulated versus experimental reported in literature; $R^2 = .36$ and .51, including and excluding juvenile yield below 6 t/ha, respectively

in research plots, and more likely related to scale and lack of spatial detail in climate and soil data.

Projections of mean annual miscanthus yields at global and UK scale (2090–2099) show considerable differences from a historic baseline (Figure 13) with spatial yield increases changing from southward to westward for the United Kingdom, and global increases in potential. In the United Kingdom, future yield projections show temperature effects enabling miscanthus production further north than possible in the 20th century. Precipitation effects indicate a restricted production without irrigation in the southeast of England, drought years decrease the potential mean annual yield, so that non-irrigated production of $M \times g$ would not be viable in the south-east under the RCP 2.6 scenario.

Figures 14 and 15 show the resulting complement of projections at United Kingdom and global scales for 2090–2099, the pattern of energy generation follows yield (Figures 14a,b and 15a,b), and CO_2 will display an inverse pattern from soil C (Figures 14c,d and 15c,d). The complementary output of miscanthus yield with electricity

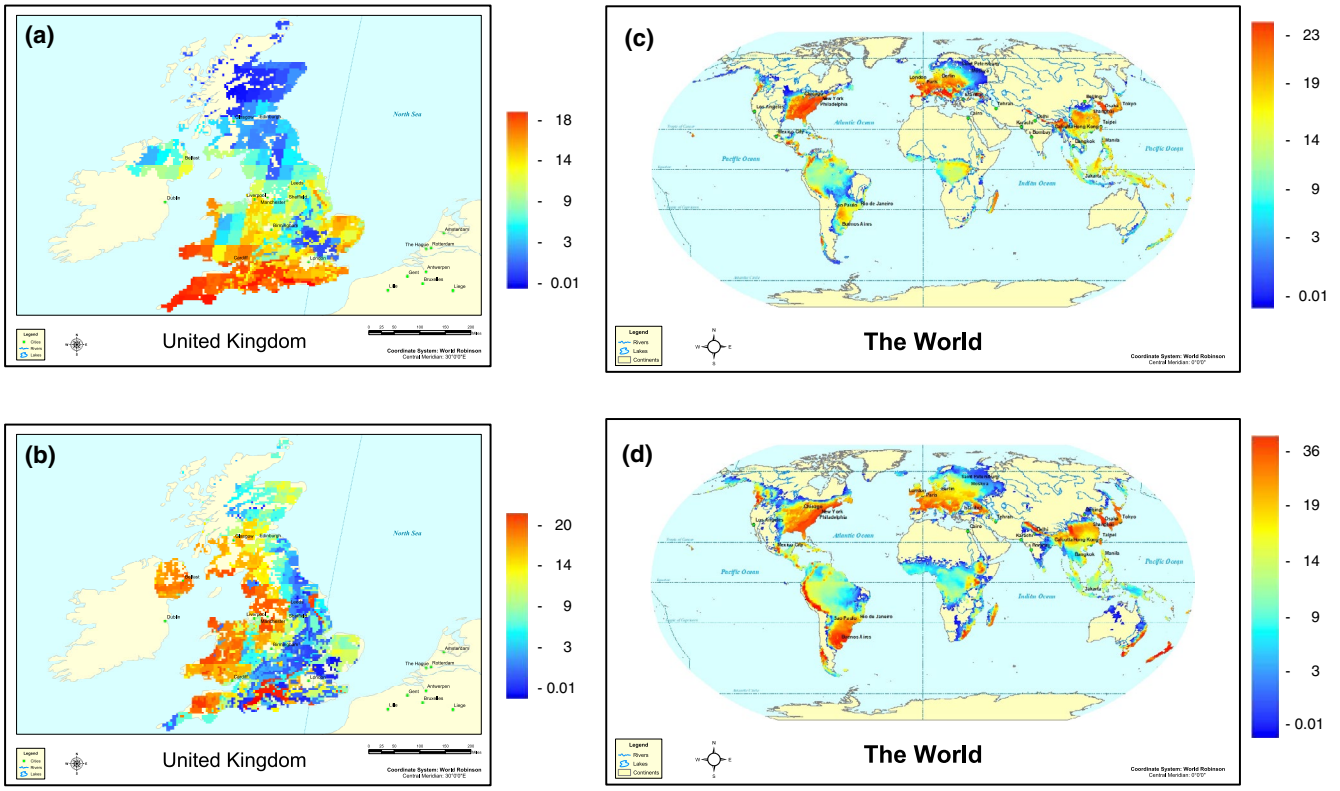

FIGURE 13 Miscanthus dry matter yield, t ha^{-1} year^{-1}; (a, c) 1961–1990 under historic climate, (b, d) 2090–2099 under RCP 2.6 climate projections

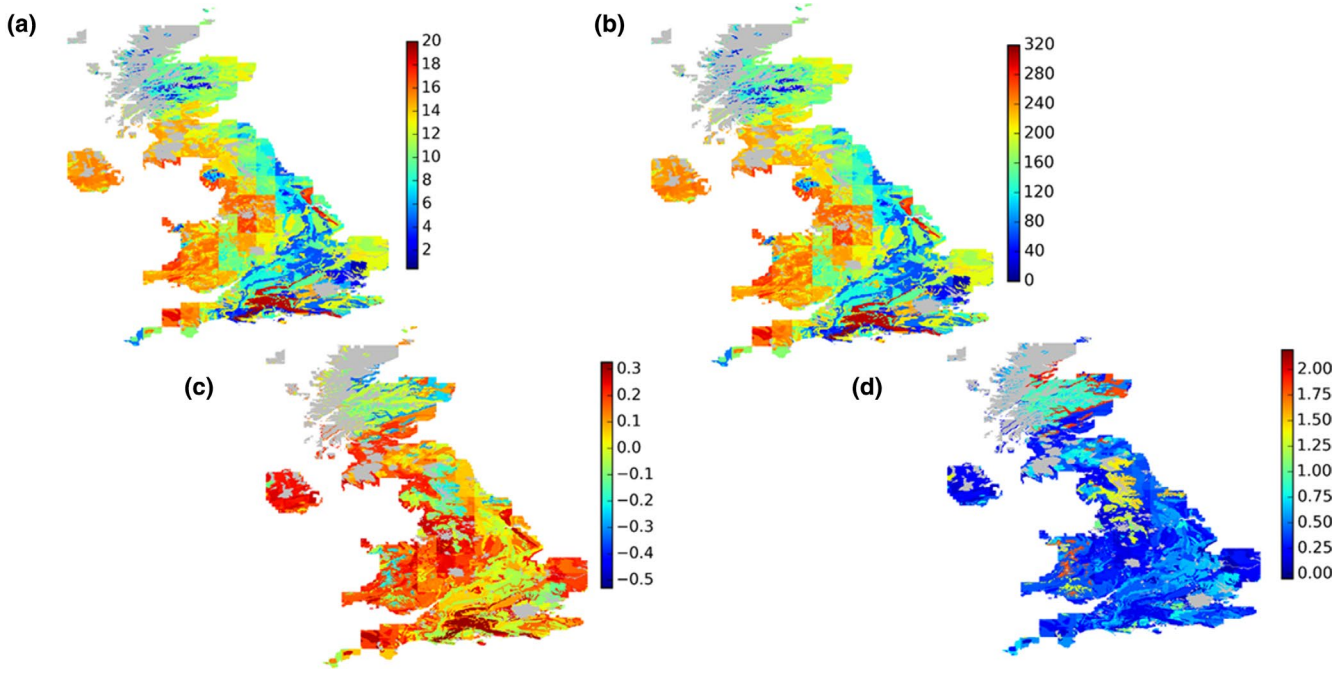

FIGURE 14 Suite of UK projections 2090–2099 for (a) dry matter yield* (b) net energy** (c) soil C change*** (d) ****CO_2. *yield in t ha^{-1} year^{-1}, **net power generated in GJ ha^{-1} year^{-1}, ***soil C change in t ha^{-1} year^{-1}, ****CO_2 emitted via processing and transport minus soil C change, expressed in CO_{2eq} in t ha^{-1} year^{-1}

generated and C consequences gives an overall view of bioenergy for miscanthus under same simulation conditions. Projections for the last decade of the 21st century indicate that in the United Kingdom, the climate will support miscanthus production of 12–20 t ha^{-1} year^{-1} with associated energy production of 200–320 GJ ha^{-1} year^{-1},

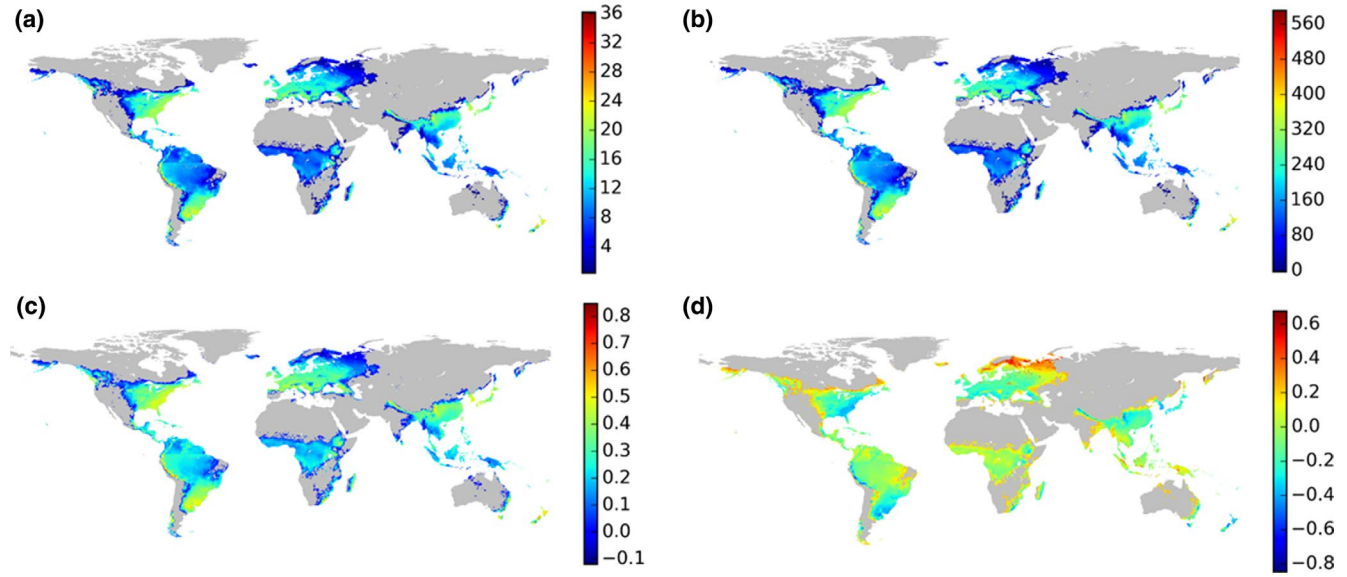

FIGURE 15 Suite of global projections 2090–2099 for (a) dry matter yield* (b) net energy** (c) soil C change*** (d) ****CO_2. *yield in t ha^{-1} $year^{-1}$, **net power generated in GJ ha^{-1} $year^{-1}$, ***soil C change in t ha^{-1} $year^{-1}$, ****CO_2 emitted via processing and transport minus soil C change, expressed in CO_{2eq} in t ha^{-1} $year^{-1}$

TABLE 2 UK mean annual projections under SSP2: simulated miscanthus dry matter yield, power generation and soil C

Projection	IAM-predicted crop area (ha)	Mean Crop Yield (dry matter biomass) (t ha^{-1} $year^{-1}$)	Total crop yield (dry matter biomass) (Gt/year)	Mean energy generated[c] (GJ ha^{-1} $year^{-1}$)	Total energy generated[c] (EJ/year)	Mean soil C gain under miscanthus (t C ha^{-1} $year^{-1}$)	Total soil C gain under miscanthus (Mt C/year)	Total C capture[d] CCS plus soil sequester (Mt C/year)
2040–2049[a]	77,580	12.89 (S.D. 4.29)	0.001	204.53	0.009	0.19	0.015	0.47
2090–2099	1,894,563	12.14 (S.D. 5.38)	0.023	192.21	0.368	0.08	0.143	10.49
Mean 21st C 2040–2099[b]	468,019	12.82 (S.D. 3.65)	0.006	203.36	0.090	0.18	0.087	2.79

[a]Earliest period of substantial bioenergy area in the United Kingdom under SSP2 land use projection.

[b]Full simulation period.

[c]Biomass heat generation, based on an assumed energy yield of 18 GJ/t of dry matter minus latent heat of vapourization at 2.72 GJ/t of moisture content (30% of dry matter weight), minus fixed energy cost (5.64 GJ/year) of crop establishment, minus energy input 0.61 GJ/t per dry matter yield (fertilizer, harvesting, transport; Hastings et al., 2008, incorporating parameters from Clifton-Brown et al., 2002; Lai, 2004).

[d]Assumed 90% CO_2 capture post-combustion (Albanito et al., 2019).

positive soil C change and relatively low C dioxide emission (from crop, soil and energy production) in Ireland and south-east Scotland, in addition to the north-west, west and south-west of England and chalk areas of the south and east. Global projections for the same decade show a much higher values per hectare as the most promising areas for miscanthus (north-eastern United States and south-eastern Canada, Brazil, southern Europe and south-east Asia) show that the climate will support 20–36 t ha^{-1} $year^{-1}$ with associated energy generation of 320–560 GJ ha^{-1} $year^{-1}$, positive soil C change and relatively low CO_2 emissions.

Tables 2 and 3 show the aggregated United Kingdom and global totals projected for miscanthus dry matter yield, simulated electricity generation and soil C change, while Table 4 shows nations with the largest potential for bioenergy.

From the IMAGE land use projections, global use of bioenergy crops starts in the early 21st century, so aggregated yield and energy generation can be calculated as early as 2010–2019, whereas the UK projections are not showing any bioenergy land use until 2040. This is not realistic, since UK bioenergy is currently being produced; however, the IAM locations are calculated on the basis of sufficient policy, economic support and infrastructure being in place, which it has determined will occur in the United Kingdom from 2040, which is the first aggregated UK projection we can determine.

TABLE 3 Global mean annual projections under SSP2: simulated miscanthus dry matter yield, power generation and soil C

Projection	IAM-predicted crop area (ha)	Mean Crop Yield (dry matter biomass) (t ha^{-1} year^{-1})	Total crop yield (dry matter biomass) (Gt/year)	Mean energy generated[c] (GJ ha^{-1} year^{-1})	Total energy generated[c] (EJ/year)	Mean soil C gain under miscanthus (t C ha^{-1} year^{-1})	Total soil C gain under miscanthus (Mt C/year)	Total C capture[d] CCS plus soil sequester (Mt C/year)
2010–2019[a]	7,508,532	8.79 (S.D. 2.66)	0.066	136.61	1.028	1.30	9.744	39.44
2090–2099	193,912,063	8.87 (S.D. 2.99)	1.720	137.90	26.742	0.22	42.897	816.90
Mean 21st C 2010–2099[b]	127,040,195	8.21 (S.D. 2.99)	1.043	127.05	16.131	0.58	73.697	543.05

[a]Earliest period of substantial bioenergy area globally under SSP2 land use projection.

[b]Full simulation period.

[c]Biomass heat generation, based on an assumed energy yield of 18 GJ/t of dry matter minus latent heat of vapourization at 2.72 GJ/t of moisture content (30% of dry matter weight), minus fixed energy cost (5.64 GJ/year) of crop establishment, minus energy input 0.61 GJ/t per dry matter yield (fertilizer, harvesting, transport; Hastings et al., 2008, incorporating parameters from Clifton-Brown et al., 2002; Lai, 2004).

[d]Assumed 90% CO_2 capture post-combustion (Albanito et al., 2019).

TABLE 4 Five highest yielding countries, annual values averaged over 2010–2099[a] and 2090–2099[a]

TOP 5 highest national yields averaged over 2005–2099[a]					TOP 5 highest national yields averaged over 2090–2099[a]				
Country	Total crop yield[b] (Gt/year)	Total energy generated[c] (EJ/year)	Total soil C gain (Mt/year)	Total C capture[d] (Mt/year)	Country	Total crop yield[b] (Gt/year)	Total energy generated[c] (EJ/year)	Total soil C gain (Mt/year)	Total C capture[d] (Mt/year)
Brazil	0.193	2.900	41.083	129.93	Brazil	0.304	4.551	15.837	152.64
Myanmar	0.076	1.182	3.124	37.32	China	0.140	1.199	9.765	72.77
Venezuala	0.064	0.995	4.249	33.05	Venezuala	0.109	1.693	1.621	50.67
Laos	0.057	0.898	1.394	27.04	Myanmar	0.096	1.492	1.162	44.36
China	0.055	0.854	25.947	50.70	USA	0.094	1.492	16.802	59.10

[a]Influenced by area under SSP2 projection for bioenergy land use.

[b]Based on crop area under IAM-generated SSP2 bioenergy.

[c]Biomass heat generation, based on an assumed energy yield of 18 GJ/t of dry matter minus latent heat of vapourization at 2.72 GJ/t of moisture content (30% of dry matter weight), minus fixed energy cost (5.64 GJ/year) of crop establishment, minus energy input 0.61 GJ/t per dry matter yield (fertilizer, harvesting, transport; Hastings et al., 2008, incorporating parameters from Clifton-Brown et al., 2002; Lai, 2004).

[d]C captured equals 90% CO_2 capture post-combustion (Albanito et al., 2019) plus soil sequestration.

We have concentrated on the increase in bioenergy from early century to late century. Supplemental Data file S1 contains projected country and global totals for biomass and power generation for all decades.

4 | DISCUSSION

4.1 | Assumptions inherent in bioenergy land use locations

This paper reports on the modification and validation of the MiscanFor model and its use to assess the potential contribution that $M \times g$ could make globally to satisfy the BECCS requirements for decarbonization associated with the RCP 2.6 climate projections. As with any model, some assumptions are inherent from the data used. We accept that the global locations used for bioenergy crop production are not always accurate. Our model does not determine land use. The land use data used for input came from data produced for a separate published study (Vaughan et al., 2018) which reviewed the global land use output by the integrated assessment model IMAGE (van Vuuren et al., 2017) as being globally acceptable in its projections, considering it to be consistent with current relevant literature.

Further details of the land use are contained in the supplemental data to the Vaughan et al. (2018) study. In scenarios used by Vaughan et al., half of the global biomass resource is derived from agricultural and forestry residues and half from dedicated bioenergy crops grown on abandoned agricultural land and expansion into grasslands. The aim of our study is to investigate how much crop and energy yield could be supplied

by this land area using *Miscanthus* × *giganteus* only to satisfy the IPCC SSP2 scenario. An example of the errors inherent in these assumptions can be seen, for example, in projections for China. Vaughan et al. land use projections indicate a change in land use over China of 1,088 Mha, we acknowledge that this was mainly from forestry and not from bioenergy crops. While the assumption is that bioenergy resources will be from converted waste land and converted grassland, much of China's waste land, for example, desert regions in Mongolia, may be too dry to grow bioenergy crops, but the bioenergy land use data produced for the Vaughan et al. (2018) study indicates locations for which climate and soil data result in sustained bioenergy crop growth. The online Atlas of Aridity (Cherlet et al., 2018) defines the eastern and central regions of China as humid rather than arid or semi-arid. Our model biomass has validated satisfactorily using data from various countries and climates, and our input climate and soil databases produce reasonable results for evapotranspiration and little crop kill due to drought for the eastern half of China. We acknowledge this may not be where the majority of waste lands are located, but the land use location data have been taken from that published by the Vaughan et al. (2018) study, we deduce that the majority of areas in this region must be converted grassland, whilst acknowledging that being dependent on an external resource to provide land use area is an assumption that can introduce error.

4.2 | Assumptions inherent in modifications for climate, crop and soil water

Simulation of crop death by drought is dependent on the AWC of the soil database (field capacity minus permanent wilting point). Calculated AWC values from the HWSD database (Figure 5a) display the lowest UK water capacity over south-eastern English soils and soils over the Scottish Highlands. AWC differences between both databases (Figure 5b) display equal areas over the United Kingdom for which each database is slightly higher in AWC than the other. HWSD water capacity is shown to be higher than IGBP over eastern Scotland and in areas of central, north-west and south-east and southwest England. Meanwhile, IGBP data have a higher AWC over upland areas of the Pennines and west of Scotland. This comparison of the soil data is something to consider if viewing results of drought and crop death. Only the dominant HWSD soil is considered, whereas in reality there can be up to 10 soil types in a 30 arc-sec grid square of the database.

The distribution of wind and its effect on higher ET_c and lowering crop water is an assumption embedded in the climate data, to consider when viewing results. Mean ET_c produced by Penman–Monteith and Thornthwaite procedures reasonably compared albeit with a spread of data (r^2 .49, rmse 79.9, $n = 842{,}043$).

The temperature modification with increasing elevation has the effect of lowering temperature for growth and also lowering ET_c, which may decrease or increase upland yield depending on temperate or tropical climate and elevation. The groundwater support has made further contrasts between areas with support and those without. The combination of adiabatic modification and groundwater support contributes to regional yield refining and produces a more detailed map (Figure 7).

4.3 | Miscanthus effects on carbon

Soil C simulated using the Bosatta and Agren procedure compared satisfactorily with experimental values from literature (Figure 8). Under miscanthus cropping, a map of soil C change (Figure 9) displays the contrast between C loss on peatland soils, and C sequestration on lower C arable soils, corresponding to known soil processes (Bot & Benites, 2005; Ontl & Schulte, 2012). Arable cropping of any crop on a high C soil risks losing more C than can be replaced, whilst on a lower C soil, miscanthus is rarely disturbed and has time to build up C stocks. Litter drop and root exudates are a function of miscanthus yield and biomass and will build over time (McCalmont et al., 2017). The simulated mean annual change in soil C under a miscanthus crop agrees with results from a review of experimental studies (McCalmont et al., 2017) which concluded a change of 0.7–2.2 Mg C4-C ha^{-1} $year^{-1}$. The McCalmont et al. review concluded that a transition to a miscanthus crop from long-term grassland would initially lose C associated with tilling, but that a long-term miscanthus crop would allow the C to increase again to a similar level. The transition from arable soils, however, resulted in soil C levels increasing, associated with the large amount of plant litter from miscanthus plus the elimination of tilling decreasing soil C decomposition. The ELUM project based on the ECOSSE model reported the same effects from its simulations (Pogson et al., 2016).

Using constraints described by Lovett, Sünnenberg, and Dockerty (2014; for high organic C soils, urban areas, outstanding beauty, designated scientific interest areas and national parks, etc.), Milner et al. (2016) suggest that if the UK land without constraints were planted with miscanthus, 99.6% would see net gains in SOC between 1.5 and 2.5 Mg C ha^{-1} $year^{-1}$. Given that the only substantial negative SOC changes in Figure 9 are located on uplands of high C soils, our simulation for 2010–2019 agrees with this finding, although we caution that the potential for soil C storage under miscanthus largely depends on the land use system it is replacing (Dondini et al., 2009; Holden et al., 2019).

We cannot realistically validate the map of CO_2 emission (Figure 10) associated with the simulation of SOC change, but it is shown for info as it is a direct consequence of the SOC results, the emission of CO_2 being in ratio with the loss of total soil C and vice versa. Hence, it shows highest emissions over

uplands and other organic or waterlogged soils, which come under the excluded areas for bioenergy (Lovett et al., 2014).

4.4 | Simulations of miscanthus yields and energy generation and CCS at global and UK scale

In developing MiscanFor, Hastings et al. (2009) added photoperiod and drought stress. In this next phase of development, a substantial amount of modification for this study was involved with crop and soil water, and its effect on photosynthetic production. Simulated yields overestimate the lowest range of observed yield, reducing the correlation of simulated-observed comparison, whereas most yields between 10 and 25 t ha^{-1} $year^{-1}$ agree satisfactorily. Low observed yield includes young rhizomes which have not yet built up the root mass to support a higher yield. The model does not include young rhizome yield increase, and this will be a necessary adjustment to the model. A concurrent project has taken field measurements for this purpose, and a publication on the modification of MiscanFor to incorporate early growth is forthcoming (Shepherd, Clifton-Brown, Buckby, & Hastings, 2019).

Although Figure 11 does not show radical differences, it does show either higher yields or an increased area of growth as a result of an increase to the leaf overheating temperature. The importance of this figure is that although we show high temperatures globally limiting the most commonly grown miscanthus variety, there are other varieties in existence such as *M. sinensis*, and new varieties being trialled which can withstand higher temperatures (Clifton-Brown et al., 2001; Clifton-Brown, Lewandowski, Bangerth, & Jones, 2002). These have the potential to increase yields in warmer humid locations.

Yield projections for 2090–2099 show considerable change since a historic baseline of 1962–1990 (Figure 13). Pogson et al. (2012) used the previous version of MiscanFor for the United Kingdom with the same HWSD soil database and CRU TS 3.0 historical climate and found similar UK yields but projected a wide region of drought-killed crops in south-east England and higher yielding regions in the north and west. This study has obtained a similar yield range as Pogson et al. but has reduced the overestimation of crop kill by drought and obtained a more realistic historic countrywide growth potential of miscanthus. UK drought crop kill is reduced to areas around greater London, under the RCP 2.6 future climate. Global yield projections show an increase over historic values, and an expansion into new regions such as Australia and New Zealand.

Thus far, maps have illustrated the suitability of all locations for miscanthus production based solely on climate and soil data. The next step is to bring in locational data from an IAM. By doing so we add a layer of data from an analysis of socio-economics and policies. The IMAGE IAM has produced SSP2 bioenergy gridded land use data, providing the area of bioenergy for CCS required to reduce GHGs, to constrain global temperature increase to within 2°C under the RCP 2.6 scenario and made locational decisions of where to place the bioenergy land use. The bioenergy land use grid is chosen on socio-economic–policy considerations and relieves the model user of locational decisions. It is also dynamic, reflecting a ramp up of bioenergy land use through the 21st century. Aggregated national or global bioenergy values based on SSP2 land use projections can now be calculated (Tables 2, 3 and 4).

UK growth projections of 77,580–1,894,563 ha of bioenergy crop in the United Kingdom (2040s to 2090s) experience positive soil C accumulations. Mean crop yields for the United Kingdom at 2050 (12 t ha^{-1} $year^{-1}$) are similar to the previous version of the model (11.9 t ha^{-1} $year^{-1}$; Hastings et al., 2014); however, we have added realistic processes with more parameters and have honed the detail of the model this is reflected in maps showing differences in detailed areas (Figure 7). Mean crop yield, energy generated and soil C increase per unit area are projected to remain stable through the 60 years due to climate variation and reduction of precipitation. Yield variation per unit area over the 21st century occurs globally (illustrated for China, Figure 16).

Due to the projected increase in bioenergy area from 77,580 to 468,019 ha, aggregated totals of UK miscanthus crop yield will grow from 0.001 to 0.023 Gt/year, mean biofuel energy will grow from 0.009 to 0.368 EJ/year and total soil C stored will increase from 0.015 to 0.143 Mt/year from the 2040s to the 2090s. This produces a C capture potential growing from 0.47 to 10.49 Mt C/year.

The global projections throughout most of the 21st century (2010s to 2090s) show an increase in bioenergy crop area of 7.5–193 million ha, a global increase in bioenergy crop yield of 0.07 to 1.72 Gt/year, bioenergy generation from 1 to 26 EJ/year, and total soil C stored increasing from 9.7 to 42.9 Mt/year. This produces a C capture potential growing from 39 to 817 Mt C/year.

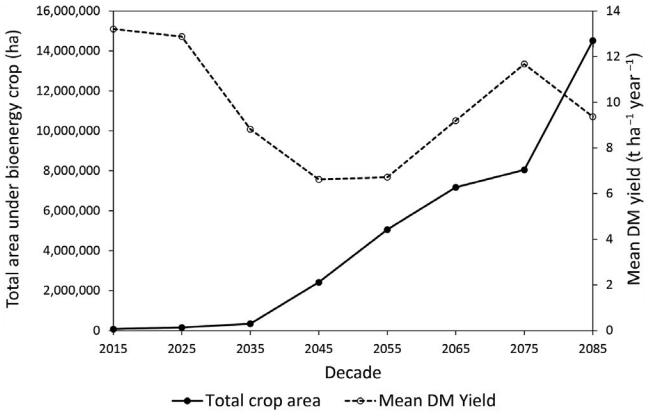

FIGURE 16 National yield influenced by climate and bioenergy area under SSP2 land use, using China as example

Again, the variable climate under RCP 2.6 is the source of variable yields (Figure 16), hence from the 2010s to 2090s, yield and energy per unit area do not show large increases, soil C storage potential decreases and aggregated increases are due to the increased area of bioenergy land use.

RCP 2.6 scenarios rely on mitigation implicit within SSP scenarios, and limit warming to below 2°C with a greater than 66% probability (IPCC, 2014). RCP 2.6 with SSP assumptions have been created by several IAMs. IAMs are fundamental in transferring socio-economic information to land use area, from which crops, bioenergy and environmental C can be modelled. IAMs typically assume an increase in mean global yield through the century and a large CCS potential (Committee for Climate Change, 2018). Yet this study's results show relatively low global mean yields which under RCP 2.6 climate stay relatively stable throughout the latter 21st century. However, the IAMs include a notional improvement in yield through breeding which is not considered in the process-based MiscanFor model. Under RCP scenarios, for global warming to remain under 2°C, 616 Gt CO_2 needs to be removed from the atmosphere by 2100 in an energy-only C budget (Mander et al., 2016) and BECCS is the dominant method used by the scenarios. The technically feasible potential for BECCS is estimated at 10 Gt CO_2/year (and 47 EJ of primary energy from biomass) by 2050 for a dedicated biomass and CCS program (International Energy Agency for GHG, 2011) as cited by Mander et al. (2016). The economic potential in the IAM, however, is assumed to be much less at 3.5 Gt CO_2/year in 2050 with 20 EJ of primary energy from biomass. Converting our C capture projections plus soil sequestration to CO_2 equivalent (via 44:12 mol. wt. ratio), MiscanFor estimates a 21st-century global CCS mean of 2.0 Gt CO_2/year with 16 EJ/year energy from biomass, rising to 3.0 Gt CO_2/year with 26 EJ/year energy for 2090–2099. Our global energy and BECCS projections agree satisfactorily with IEA (2011). Mander et al. suggest that for RCP 2.6 to be a feasible reduction of global warming to under 2°C, 70 EJ of global bioenergy are required by 2050. It concludes this is higher than the IEA-stated feasibility, and our study supports this finding.

Other studies may not have specifically simulated miscanthus under RCP 2.6 climate with SSP2 bioenergy land use designated areas for aggregated totals, so may vary compared to ours with respect to bioenergy yields. Under SSP2 bioenergy land use, the global bioenergy calculated in our study for 2010–2019 is 1.028 EJ/year. WEA (2000) estimated that 0.6 EJ/year electricity and 2.5 EJ/year heat were being produced globally in 2000 from bioenergy. The International Energy Agency for Bioenergy (2007) assessed from a review of literature that, with an assumption of 1–2 Gha of land area for bioenergy farming on agricultural land, and an average yield of 8–12 t ha^{-1} $year^{-1}$, the energy production up to 2050 would be 100–300 EJ/year. 2 Gha land area is 20 times the SSP2 land area at the end of the century of 0.19 Gha, but pro-rata the energy production of 100–300 EJ/year becomes 20 EJ/year close to our global bioenergy projections of 16 EJ/year as a 90 year average. Our global yield per unit area projection also agrees with their lower estimation of 8 t ha^{-1} $year^{-1}$, this appears to be a relatively low yield but the SSP2 locational choice for bioenergy land use has not been made on a high yield basis.

Globally, the highest yielding countries will be those with the most suitable climates for miscanthus, or the largest land use area. The highest national yields vary through the century with the boost in bioenergy land use area under the IAM-SSP2 scenario (shown in Table 4 for 2010–2090 and 2090–2099). By the final decade of the century, the United States will have the potential to be a major bioenergy provider (1.5 EJ/year energy; 16.8 Mt/year soil C storage; 0.2 Gt CO_2 capture/year), but on average for 2010–2090, the four countries with the greatest aggregated potential are Brazil (2.9 EJ/year energy; 41 Mt/year soil C storage; 0.47 Gt CO_2 capture/year), Myanmar (1.2 EJ/year energy; 3.1 Mt/year soil C storage; 0.14 Gt CO_2 capture/year), Venezuela (1.0 EJ/year energy; 4.2 Mt/year soil C storage; 0.12 Gt CO_2 capture/year) and China (0.85 EJ/year energy; 26 Mt/year soil C storage; 0.18 Gt CO_2 capture/year). Of these Brazil and China are also the nations with the most bioenergy land area. Hastings et al. (2008) mention the global increase of energy due to the rapid industrialization of the economies of South East Asia, Brazil, China. It seems fortunate that these countries are the ones with the projected potential to support their industrialization with bioenergy. Ranked countries highlight a weakness with the socio-economic forecasting of the IAM-derived global bioenergy locations. Venezuela has globally the second largest oil reserves and a very poor and underdeveloped agricultural sector, little incentive to build the capacity to produce 109 Mega tonnes/year crop yield, so it is surprising to see it ranked highly based on the bioenergy land use area.

Pogson, Hastings, and Smith (2013) projections calculated Asia as the largest miscanthus supplier of bioenergy from crops. China has the largest miscanthus growth area worldwide at present, with approximately 100,000 ha, varieties largely based on wild *M. lutarioriparius* with a yield potential of 12 t ha^{-1} $year^{-1}$ (Xue, Xiao, & Zili, 2015). A review of bioenergy potentials (Smeets, Lewandowski, & Turkenburg, 2007) gave S America and Caribbean, sub-Saharan Africa, Oceania and America as countries with the most bioenergy potential on surplus land. This shows agreement with our study for major potential bioenergy production areas of the world (Figure 15 and Table 4).

A plot of global totals through the decades (Figure 17) shows a clear increase in global biomass and power generation, plus a gentle increase in the standard deviation of global biomass values over 10 years. The continual increase in all three relate to the land use area, as the initial ramp-up of bioenergy from 2040, shows an acceleration of global totals, so noticeably does the last decade. The increase in the standard deviation of the biomass will be driven by a variation in soil

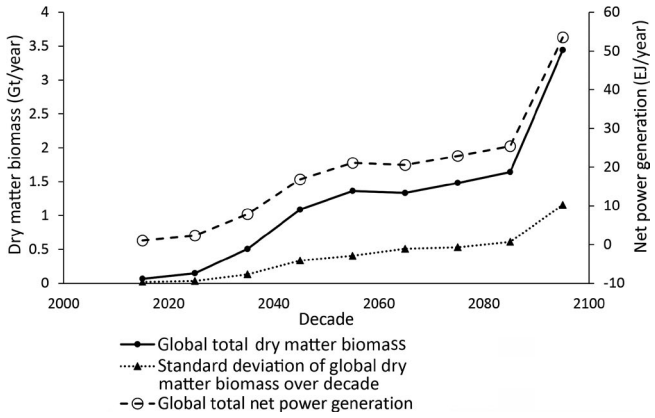

FIGURE 17 Global totals through the decades, dry matter biomass and power generation, plus biomass standard deviation

type and climate with increasing land area. The climate of the additional land use areas will modify the rate of increase for each decade.

All country and global projected totals for biomass and energy generation for all decades since 2010–2090 have been provided in Supplemental Data file S1.

We caution that our simulations are for a mature miscanthus crop, and do not include emissions resulting from past land use conversion. Holder et al. (2019) modelled miscanthus, underpinned by experimental soil C change, and concluded that C change is dependent on former land use. Converting grassland to miscanthus can increase global warming potential during the first 15 years. Vaughan et al. (2018) investigated the BECCS assumptions relating to low emission scenarios, including biomass resource and land use. Like Holder et al., they report that half of the projected biomass is derived from dedicated bioenergy crops grown on abandoned agricultural land and expanded into grasslands, but that poor governance to prevent higher C grassland conversion in most regions with high growth potential will limit the BECCS potential for CO_2 removal, offset by land use change emissions and lower soil C.

Also, projections for the yield, electricity generation and effects on C and C captured have been projected, to show the potential of miscanthus using the variety $M \times g$. A model is a simplistic representation of a complex system. In reality, different varieties of miscanthus will be grown, best suited to local climate conditions, and either further development of this model or an IAM-derived land use could display several bioenergy feedstock resources, with crop varieties grown for location dependent on best suitability for the climate (Clifton-Brown et al., 2019).

In summary, modifications to MiscanFor were made to correct the sensitivity of yields to drought, and overestimation of yield at low latitudes. We have had to balance drought risk against more realistic crop and water processes that we invoked, some which can restrict water further (downregulation), some which can ease water restriction (evapotranspiration replacement using more climate inputs and groundwater support). New climate, soil, groundwater and land use data sets have underpinned these modifications. At fine-scale resolution, further spatial distinction was possible allowing regional details to emerge whose patterns were influenced by soil types and drainage basins on top of climate.

Projections show a boost in global bioenergy land use, creating a surge in bioenergy to 26.7 EJ/year by the 2090s, with the foremost national providers projected to be Brazil and China based on land area, high yielding crops and soil C increase, although the United States is projected to have that capability later in the century. Our projections of global miscanthus yield per unit area, global energy (2005–2009) pro-rated with land use area and 21st-century projections of aggregated global energy and CCS are all consistent with those of published studies. Our results indicate insufficient global CCS projections using miscanthus for the SSP2 CCS requirements. The global land area needed to produce the amount of bioenergy required to satisfy the RCP 2.6 projections, based solely on miscanthus, would have to be about 19 times larger unless a higher yielding crop was found. Conversely, this also means that miscanthus can provide just over 5% of the global energy needs. This agrees with the lower limit from Hastings et al. (2008) assessment that miscanthus could provide between 5% and 15% of Europe's primary energy needs by 2080 if considered to be the only bioenergy crop. In reality, miscanthus will be one of several bioenergy crops increasing in production this century, others will be better suited to regional climates than miscanthus, and this will increase the mean bioenergy and CCS. It also highlights the global need for ongoing improvement in miscanthus and other bioenergy crops in breeding and field equipment, plus the global need for more infrastructure and miscanthus supply chain specialists supporting growers to increase the uptake and investment in bioenergy crops.

ACKNOWLEDGEMENTS

This work is part of FAB GGR (Feasibility of Afforestation and Biomass energy with carbon capture and storage for Greenhouse Gas Removal), a project funded by the UK Natural Environment Research Council (NE/P019951/1), part of a wider Greenhouse Gas Removal research programme (http://www.fab-ggr.org/). This work forms part of the ADVENT project funded by the UK Natural Environment Research Council (NE/M019691/1) and the Assess-BECCS funded by EPSRC via UKERC. We would also like to thank Detlef van Vuuren who via the FAB GGR project provided the SSP2 land use projections for bioenergy created by IMAGE integrated assessment model.

ORCID

Anita Shepherd https://orcid.org/0000-0003-1902-5147
John Clifton-Brown https://orcid.org/0000-0001-6477-5452

REFERENCES

Albanito, F., Hastings, A., Fitton, N., Richards, M., Martin, M., MacDowell, N., … Smith, P. (2019). Mitigation potential and environmental impact of centralized versus distributed BECCS with domestic biomass production in Great Britain. *GCB Bioenergy*, *11*, 1234–1252. https://doi.org/10.1111/gcbb.12630

Allen, R. G., Pereira, L. S., Raes, D., & Smith, M. (1998). *Crop evapotranspiration – Guidelines for computing crop water requirements – FAO Irrigation and drainage paper 56*. Rome, Italy: FAO.

Bosatta, E., & Agren, G. I. (1985). Theoretical analysis of decomposition of heterogeneous substrates. *Soil Biology and Biochemistry*, *17*, 601–610.

Bosatta, E., & Agren, G. I. (1991). Dynamics and carbon and nitrogen in the organic matter of the soil: A generic theory. *The American Naturalist*, *138*, 227–245.

Bot, A., & Benites, J. (2005). *The importance of soil organic matter. Key to drought-resistant soil and sustained food production. FAO Soils Bulletin 80*. Rome, Italy: FAO.

Cherlet, M., Hutchinson, C., Reynolds, J., Hill, J., Sommer, S., & von Maltitz, G. (Eds.). (2018). *World atlas of desertification*. Luxembourg: Publication Office of the European Union.

Clifton-Brown, J. C., Breuer, J., & Jones, M. B. (2007). Carbon mitigation by the energy crop Miscanthus. *Global Change Biology*, *13*, 2296–2307.

Clifton-Brown, J., Harfouche, A., Casler, M. D., Jones, H. D., Macalpine, W. J., Murphy-Bokern, D., … Lewandowski, I. (2019). Breeding progress and preparedness for mass-scale deployment of perennial lignocellulosic biomass crops switchgrass, miscanthus, willow and poplar. *GCB Bioenergy*, *11*, 118–151. https://doi.org/10.1111/gcbb.12566

Clifton-Brown, J. C., Lewandowski, I., Andersson, B., Basch, G., Christian, D. G., Kjeldsen, J. B. … Teixeira, F. (2001). Performance of 15 Miscanthus Genotypes at five sites in Europe. *Agronomy Journal*, *93*, 1013–1019. https://doi.org/10.2134/agronj2001.9351013x

Clifton-Brown, J. C., Lewandowski, I., Bangerth, F., &Jones, M. B. (2002). Comparative responses to water stress in stay-green, rapid- and slow senescing genotypes of the biomass crop, Miscanthus. *New Phytologist*, *154*, 335–345.

Collins, W. J., Bellouin, N., Doutriaux-Boucher, M., Gedney, N., Halloran, P., Hinton, T., … Woodward, S. (2011). Development and evaluation of an Earth-System model – HadGEM2. *Geoscientific Model Development*, *4*, 1051–1075. https://doi.org/10.5194/gmd-4-1051-2011

Committee on Climate Change. (2018). Biomass in a low energy economy. © Committee on Climate Change Copyright. Retrieved from https://www.theccc.org.uk/wp-content/uploads/2018/11/Biomass-in-a-low-carbon-economy-CCC-2018.pdf

Daioglou, V., Doelman, J. C., Wicke, B., Faaij, A., & van Vuuren, D. P. (2019). Integrated assessment of biomass supply and demand in climate change mitigation scenarios. *Global Environmental Change*, *54*, 88–101. https://doi.org/10.1016/j.gloenvcha.2018.11.012

Doelman, J. C., Stehfest, E., Tabeau, A., van Meijl, H., Lassaletta, L., Gernaat, D. E. H. J., … van Vuuren, D. P. (2018). Exploring SSP land-use dynamics using the IMAGE model: Regional and gridded scenarios of land-use change and land-based climate change mitigation. *Global Environmental Change*, *48*, 119–135. https://doi.org/10.1016/j.gloenvcha.2017.11.014

Dondini, M., Hastings, A., Saiz, G., Jones, M. B., & Smith, P. (2009). The potential of Miscanthus to sequester carbon in soils: Comparing field measurements in Carlow, Ireland to model predictions. *GCB Bioenergy*, *1*, 413–442. https://doi.org/10.1111/j.1757-1707.2010.01033.x

Farage, P. K., Blowers, D., Long, S. P., & Baker, N. R. (2006). Low growth temperatures modify the efficiency of light use by photosystem II for CO_2 assimilation in leaves of two chilling-tolerant C_4 species, *Cyperus longus* L. and Miscanthus × giganteus. *Plant, Cell and Environment*, *29*, 720–728.

Global Soil Data Task Group. (2000). Global Gridded Surfaces of Selected Soil Characteristics (IGBP-DIS). [Global Gridded Surfaces of Selected Soil Characteristics (International Geosphere-Biosphere Programme – Data and Information System)]. Data set. Retrieved from http://www.daac.ornl.gov from Oak Ridge National Laboratory Distributed Active Archive Center, Oak Ridge, Tennessee, U.S.A. 2018. https://doi.org/10.3334/ORNLDAAC/569

Goulding, K. W. T., Bailey, N. J., Bradbury, N. J., Hargreaves, P., Howe, M., Murphy, D. V., … Willison, T. W. (1998). Nitrogen deposition and its contribution to nitrogen cycling and associated soil processes. *New Phytologist*, *139*, 49–58.

Hager, H. A., Sinasac, S. E., Gedalof, Z., & Newman, J. A. (2014). Predicting potential global distributions of two Miscanthus grasses: Implications for horticulture, biofuel production, and biological invasions. *PLoS ONE*, *9*(6), e100032. https://doi.org/10.1371/journal.pone.0100032

Harris, I. C., & Jones, P. D. (2017). CRU TS4.01: Climatic Research Unit (CRU) Time-Series (TS) version 4.01 of high-resolution gridded data of month-by-month variation in climate (Jan. 1901- Dec. 2016). Centre for Environmental Data Analysis, 04 December 2017. https://doi.org/10.5285/58a8802721c94c66ae45c3baa4d814d0. Accessed March+ 30, 2019.

Hastings, A., Clifton-Brown, J., Wattenbach, M., Mitchell, C. P., & Smith, P. (2009). The development of MISCANFOR, a new Miscanthus crop growth model: Towards more robust yield predictions under different climatic and soil conditions. *Global Change Biology Bioenergy*, *1*, 154–170. https://doi.org/10.1111/j.1757-1707.2009.01007.x

Hastings, A., Mos, M., Yesufu, J. A., McCalmont, J., Schwarz, K., Shafei, R., … Clifton-Brown, J. (2017). Economic and environmental assessment of seed and rhizome propagated Miscanthus in the UK. *Frontiers of Plant Science*, *8*, 1058. https://doi.org/10.3389/fpls.2017.01058

Hastings, A. F., St Clifton-Brown, J., Wattenbach, M., Stampfl, P., Mitchell, C. P., & Smith, P. (2008). Potential of Miscanthus grasses to provide energy and hence reduce greenhouse gas emissions. *Agronomy for Sustainable Development*, *28*, 465–472. ffhal-00886411f.

Hastings, A., Tallis, M. J., Casella, E., Matthews, R. W., Henshall, P. A., Milner, S., … Taylor, G. (2014). The technical potential of Great Britain to produce ligno-cellulosic biomass for bioenergy in current and future climates. *GCB Bioenergy*, *6*, 108–122. https://doi.org/10.1111/gcbb.12103

Hempel, S., Frieler, K., Warszawski, L., Schewe, J., & Piontek, F. (2013). Bias corrected GCM input data for ISIMIP Fast Track. *GFZ Data Services*, https://doi.org/10.5880/PIK.2016.001

Holder, A. J., Clifton-Brown, J., Rowe, R., Robson, P., Elias, D., Dondini, M., … McCalmont, J. (2019). Measured and modelled effect of land use change from temperate grassland to Miscanthus on soil carbon stocks after 12 years. *GCB Bioenergy*, *11*(10), 1173–1186. https://doi.org/10.1111/gcbb.12624

International Energy Agency for Bioenergy. (2007). Potential contribution of bioenergy to the world's future energy demand. IEA

BIOENERGY: EXCO: 2007:02. Accessed online: 20th September, 2019. Retrieved from https://www.ieabioenergy.com/wp-content/uploads/2013/10/Potential-Contribution-of-Bioenergy-to-the-Worlds-Future-Energy-Demand.pdf

International Energy Agency for GHG. (2011). Potential for biomass with carbon capture and storage. 2011/06. Retrieved from https://www.eenews.net/assets/2011/08/04/document_cw_01.pdf

IPCC. (2007). *Fourth assessment report, climate change synthesis report*. Cambridge, UK: Cambridge University Press. Retrieved from https://www.ipcc.ch/site/assets/uploads/2018/03/ar4_wg3_full_report-1.pdf

IPCC. (2014). Representative Concentration Pathways (RCPs). IPCC Data Distribution website. Retrieved from https://sedac.ciesin.columbia.edu/ddc/ar5_scenario_process/RCPs.html

Jarvis, A., Reuter, H. I., Nelson, A., & Guevara, E. (2008). Hole-filled SRTM for the globe Version 4. Available from the CGIAR-CSI SRTM 90m Database. Retrieved from http://srtm.csi.cgiar.org

Lai, R. (2004). Carbon emission from farm operations. *Environment International*, *30*, 981–990.

Lesur-Dumoulin, C., Lorin, M., Bazot, M., Jeuffroy, M.-H., & Loyce, C. (2016). Analysis of young Miscanthus × giganteus yield variability: A survey of farmers' fields in east central France. *GCB Bioenergy*, *8*(1), 122–135. https://doi.org/10.1111/gcbb.12247

Lovett, A., Sünnenberg, G., & Dockerty, T. (2014). The availability of land for perennial energy crops in Great Britain. *GCB Bioenergy*, *6*, 99–107. https://doi.org/10.1111/gcbb.12147

Mander, S., Andersona, K., Larkin, A., Gough, C., & Vaughan, N. (2016). The role of bio-energy with carbon capture and storage in meeting the climate mitigation challenge: A whole system perspective. *Energy Procedia*, *114*, 6036–6043. https://doi.org/10.1016/j.egypro.2017.03.1739

Martin, G. M., Bellouin, N., Culverwell, W. J., Halloran, P. R., Hardiman, S. C., Hinton, T. J., … Wiltshire, A. (2011). The HadGEM2 family of Met Office Unified Model climate configurations. *Geoscience Model Development*, *4*, 723–757. https://doi.org/10.5194/gmd-4-723-2011

McCalmont, J., Hastings, A., Mcnamara, N., Richter, G., Robson, P., Donnison, I., & Clifton-Brown, J. (2017). Environmental costs and benefits of growing Miscanthus for bioenergy in the UK. *GCB Bioenergy*, *9*(3), 489–507. https://doi.org/10.1111/gcbb.12294

Meinshausen, M., Smith, S. J., Calvin, K., Daniel, J. S., Kainuma, M. L. T., Lamarque, J.-F., … van Vuuren, D. P. P. (2011). The RCP greenhouse gas concentrations and their extensions from 1765 to 2300. *Climatic Change*, *109*(1–2), 213–241. https://doi.org/10.1007/s10584-011-0156-z

Milner, S., Holland, R. A., Lovett, A., Sunnenberg, G., Hastings, A., Smith, P., … Taylor, G. (2016). Potential impacts on ecosystem services of land use transitions to second-generation bioenergy crops in GB. *GCB Bioenergy*, *8*, 317–333. https://doi.org/10.1111/gcbb.12263

Monteith, J. L. (1977). Climate and the efficiency of crop production in Britain. *Philosophical Transactions of the Royal Society of London*, *13*, 281–294.

Ontl, T. A., & Schulte, L. A. (2012). Soil carbon storage. *Nature Education Knowledge*, *3*(10), 35.

Poeplau, C., & Don, A. (2014). Soil carbon changes under Miscanthus driven by C4 accumulation and C3 decomposition-toward a default sequestration function. *GCB Bioenergy*, *6*, 327–338.

Pogson, M., Hastings, A., & Smith, P. (2012). Sensitivity of crop model predictions to entire meteorological and soil input datasets highlights vulnerability to drought. *Environmental Modelling & Software*, *29*, 37–43.

Pogson, M., Hastings, A., & Smith, P. (2013). How does bioenergy compare with other land-based renewable energy sources globally? *GCB Bioenergy*, *5*, 513–524. https://doi.org/10.1111/gcbb.12013

Pogson, M., Richards, M., Dondini, M., Jones, E. O., Hastings, A., & Smith, P. (2016). ELUM: A spatial modelling tool to predict soil greenhouse gas changes from land conversion to bioenergy in the UK. *Environmental Modelling & Software*, *84*, 458–466. https://doi.org/10.1016/j.envsoft.2016.07.011

Riahi, K., van Vuuren, D. P., Kriegler, E., Edmonds, J., O'Neill, B. C., Fujimori, S., … Tavoni, M. (2017). The Shared Socioeconomic Pathways and their energy, land use, and greenhouse gas emissions implications: An overview. *Global Environmental Change*, *42*, 153–168. https://doi.org/10.1016/j.gloenvcha.2016.05.009

Robertson, A. D., Whitaker, J., Morrison, R., Davies, C. A., Smith, P., & McNamara, N. (2017). A Miscanthus plantation can be carbon neutral without increasing soil carbon stocks. *GCB Bioenergy*, *9*, 645–661. https://doi.org/10.1111/gcbb.12397

Rogelj, J., Luderer, G., Pietzcker, R. C., Kriegler, E., Schaeffer, M., Krey, V., & Riahi, K. (2015). Energy system transformations for limiting end-of-century warming to below 1.5 ° C. *Nature Climate Change*, *5*, 519–527. https://doi.org/10.1038/nclimate2572

Schlamadinger, B., Faaij, A., Junginger, M., Daugherty, E., & Woess-Gallasch, S. (2006). Should we trade biomass, bio-electricity, green certificates or CO_2 credits? IEA Bioenergy Agreement Annual Report 2005, IEA Bio-energy; ExCo: 2006:01, January. pp. 4–19.

Shepherd, A., Clifton-Brown, J., Buckby, S., & Hastings, A. (2019). Miscanthus yields in a commercial environment. *GCB Bioenergy*, in press.

Sims, R. E. H., Hastings, A., Schlamadinger, B., Taylor, G., & Smith, P. (2006). Energy crops: Current status and future prospects. *Global Change Biology*, *12*, 2054–2076.

Smeets, E., Lewandowski, I., & Turkenburg, W. C. (2007). A bottom-up assessment and review of global bio-energy potentials to 2050. *Progress in Energy and Combustion Science*, *33*, 56–106. https://doi.org/10.1016/j.pecs.2006.08.001

St Clair, S., Hillier, J., & Smith, P. (2008). Calculating the pre-harvest greenhouse gas costs of energy crops. *Biomass and Bioenergy*, *32*, 442–452.

Stehfest, E., Van Vuuren, D. P., Kram, T., & Bouwman, A. F. (2014). Integrated Assessment of Global Environmental Change with IMAGE 3.0. Model description and policy applications, in: PBL Netherlands Environmental Assessment Agency, The Hague. Retrieved from http://themasites.pbl.nl/models/image/index.php/Main_Page

UKCP09. (2018). UK climate projections. Retrieved from http://ukclimateprojections-ukcp09.metoffice.gov.uk/24127

van Vuuren, D. P., Stehfest, E., den Elzen, M. G. J., Kram, T., van Vliet, J., Deetman, S., … van Ruijven, B. (2011). RCP2.6: Exploring the possibility to keep global mean temperature increase below 2°C. *Climatic Change*, *109*, 95. https://doi.org/10.1007/s10584-011-0152-3

van Vuuren, D. P., Stehfest, E., Gernaat, D., Doelman, J. C., van den Berg, M., Harmsen, M., … Tabeau, A. (2017). Energy, land-use and greenhouse gas emissions trajectories under a green growth paradigm. *Global Environmental Change*, *42*, 237–250. https://doi.org/10.1016/j.gloenvcha.2016.05.008

Vaughan, N. E., Gough, C., Mander, M., Littleton, E. W., Welfle, A., Gernaat, D. E. H. J., & van Vuuren, D. P. (2018). Evaluating the use of biomass energy with carbon capture and storage in low emission scenarios. *Environmental Research Letters*, *13*(4), 044014.

Supplemental data. Retrieved from https://iopscience.iop.org/1748-9326/13/4/044014/media/ERL_044014_SD.pdf

Wieder, W. R., Boehnert, J., Bonan, G. B., & Langseth, M. (2014). Regridded Harmonized World Soil Database v1.2. Data set. Retrieved from http://daac.ornl.gov from Oak Ridge National Laboratory Distributed Active Archive Center, Oak Ridge, Tennessee, USA. 2019, https://doi.org/10.3334/ORNLDAAC/1247, accessed 24th September.

World Energy Assessment. (2000). World energy assessment of the United Nations. UNDP, UNDESA/WEC, Published by: UNDP, New York, September.

Xue, S., Xiao, L., & Zili, Y. (2015). Miscanthus production and utilization in Dongting Lake Region, China. International Conference on Perennial biomass crops for a resource-constrained world. Biomass 2015. September 7–10, Stuttgart-Hohenheim, Germany.

SUPPORTING INFORMATION

Additional supporting information may be found online in the Supporting Information section.

How to cite this article: Shepherd A, Littleton E, Clifton-Brown J, Martin M, Hastings A. Projections of global and UK bioenergy potential from *Miscanthus* × *giganteus*—Feedstock yield, carbon cycling and electricity generation in the 21st century. *GCB Bioenergy*. 2020;12:287–305. https://doi.org/10.1111/gcbb.12671